EDGE ARTICLE

Check for updates

Degradable polyisoprene by radical ring-opening polymerization and application to polymer prodrug nanoparticles†

Maëlle Lages,[a] Théo Pesenti, [ID][a] Chen Zhu,[a] Dao Le,[a] Julie Mougin,[a] Yohann Guillaneuf[b] and Julien Nicolas [ID] *[a]

Radical ring-opening polymerization (rROP) has received renewed attention to incorporate cleavable linkages into the backbones of vinyl polymers, especially from cyclic ketene acetals (CKAs). Among the monomers that hardly copolymerize with CKAs are (1,3)-dienes such as isoprene (I). This is unfortunate since synthetic polyisoprene (PI) and its derivatives are the materials of choice for many applications, in particular as elastomers in the automotive, sport, footwear, and medical industries, but also in nanomedicine. Thionolactones have been recently proposed as a new class of rROP-compatible monomers for insertion of thioester units in the main chain. Herein, we report the synthesis of degradable PI by rROP *via* the copolymerization of I and dibenzo[*c*,*e*]oxepane-5-thione (DOT). Free-radical polymerization as well as two reversible deactivation radical polymerization techniques were successfully used for the synthesis of (well-defined) P(I-*co*-DOT) copolymers with adjustable molecular weights and DOT contents (2.7–9.7 mol%). Reactivity ratios of $r_{DOT} = 4.29$ and $r_I = 0.14$ were determined, suggesting preferential incorporation of DOT in comparison to I. The resulting P(I-*co*-DOT) copolymers were successfully degraded (from −47% to −84% decrease in M_n) under basic conditions. As a proof of concept, the P(I-*co*-DOT) copolymers were formulated into stable and narrowly dispersed nanoparticles, showing similar cytocompatibility on J774.A1 and HUVEC cells compared to their PI counterparts. Furthermore, Gem-P(I-*co*-DOT) prodrug nanoparticles were synthesized by the "drug-initiated" method and exhibited significant cytotoxicity on A549 cancer cells. P(I-*co*-DOT) and Gem-P(I-*co*-DOT) nanoparticles were degraded under basic/oxidative conditions by bleach and under physiological conditions in the presence of cysteine or glutathione.

Introduction

Degradable vinyl polymers are receiving considerable attention due to their application in the biomedical field (*e.g.*, safety of injected materials and facilitated excretion),[1] but also to address environmental issues (*e.g.*, environmental preservation and the circular plastic economy).[2–4] In this context, there has been a renewed interest in radical ring-opening copolymerization (rROP)[5] as a means of imparting degradability to vinyl polymers through the "cleavable comonomer" approach, particularly with cyclic ketene acetals (CKAs) which are precursors to ester groups in the polymer backbone.[6] Yet, CKAs exhibit important limitations such as: (i) a low reactivity

[a]Université Paris-Saclay, CNRS, Institut Galien Paris-Saclay, 17 Avenue des Sciences, 91400 Orsay, France. E-mail: julien.nicolas@universite-paris-saclay.fr; Web: https:// twitter.com/julnicolas; Tel: +33 1 80 00 60 81

[b]Aix-Marseille-Univ., CNRS, Institut de Chimie Radicalaire, UMR 7273, F-13397 Marseille, France

† Electronic supplementary information (ESI) available. See DOI: https://doi.org/10.1039/d2sc05316k

towards important classes of vinyl monomers (*e.g.*, acrylates, styrenics, methacrylates, *etc.*), thus requiring at best a large excess of CKAs in the comonomer feed; (ii) an often significant proportion of ring-retained CKAs during polymerization, resulting in non-degradable acetal units in the copolymer backbone and (iii) a very poor stability in protic solvents or in the presence of traces of water, thus severely limiting their use for instance in polymerization in aqueous dispersed media.[5,6]

Among the monomers that hardly copolymerize with CKAs are (1,3)-dienes such as isoprene (I). Synthetic polyisoprene (PI) and its derivatives are the materials of choice for many applications, in particular as elastomers in the automotive, sport, footwear and medical industries,[7,8] with a global PI market size estimated at USD 2.15 billion in 2020.[9] PI-based materials have also been extensively studied for application in colloids,[10–12] materials science/nanotechnology[13–16] and drug delivery owing to their biocompatibility and structural analogy with natural terpenoids.[17–22] Moreover, the inclusion of double bonds in the polymer backbone provides an opportunity for further functionalization *via* silylation or thiol-ene chemistry.[23,24] Even if PI can be degraded by thermal,[25] chemical (*e.g.*, ozone,[16,26]

chloranil,[27] periodic acid,[28] potassium persulfate,[29] Grubbs catalysts,[30,31] and photo-oxidation)[32,33] and biological (enzymatic[34–36] and bacterial)[37] pathways (although they cannot occur under healthy physiological conditions), insertion of labile functionalities into PI backbones, allowing their degradation and potential recyclability, has never been a success. DFT calculations indeed recently predicted very unfavourable reactivity ratios for the free-radical polymerization (FRP) of I with main CKAs (e.g., $r_{MDO} = 0.02$ and $r_I = 9.5$; $r_{BMDO} = 0.006$ and $r_I = 157$ at 70 °C),[38] suggesting very little incorporation of CKA units into the PI backbone. Experimental results confirmed the very low insertion of 2-methylene-1,3-dioxepane (MDO) while almost no open 5,6-benzo-2-methylene-1,3-dioxepane (BMDO) units were present. Therefore, an efficient pathway for PI degradation via rROP would certainly have major implications in many different areas such as sustainable materials and biomedical applications.

Thionolactones have been recently reported as a new class of cyclic monomers capable of polymerization by rROP and more specifically via a thiocarbonyl-addition-ring opening (TARO) mechanism, enabling insertion of labile thioester groups into the polymer backbone.[5] In particular, it has been shown that dibenzo[c,e]oxepane-5-thione (DOT) exhibited superior reactivity towards several vinyl monomers (e.g., acrylates,[39,40] acrylamides,[41] acrylonitrile,[39] styrene (S)[42] and maleimide[43]), extensive stability in protic solvents and in aqueous media, and quantitative ring opening.[39–41,43,44] Furthermore, it allows to diversify degradation pathways; from hydrolysis[41,42,44,45] to aminolysis[39–41] and thiolysis.[43] Very recently, DOT was copolymerized with nBA or S by either conventional emulsion polymerization[44] and polymerization-induced self-assembly,[46] while DOT was also used to impart chemical recyclability to polystyrene.[47] Moreover, it has been shown that DOT-containing copolymers can be degraded in the presence of physiologically relevant concentrations of cysteine or glutathione,[48] which allows DOT-containing copolymers to be considered in nanomedicine.

Herein, we report the successful rROP of I and DOT by both FRP and two reversible deactivation radical polymerization techniques: nitroxide-mediated polymerization[49] (NMP) and reversible addition–fragmentation chain-transfer[50] (RAFT) polymerization (Fig. 1). Owing to favourable reactivity ratios, we demonstrated the formation of thioester-containing copolymers that can be readily degraded under basic conditions. To show the versatility and broad applicability of this copolymerization system, we also reported the formulation of the resulting copolymers into nanoparticles as well as the synthesis of degradable polymer prodrug nanoparticles for anticancer therapy.

Experimental part

Materials

Isoprene (I, 99%), dicumyl peroxide (DCP, 98%), potassium hydroxide (KOH, 90%), dioxane (anhydrous, 99.8%) and isopropylamine (≥99%) were purchased from Sigma-Aldrich and used as received. (N-tert-Butyl-N-(1-diethoxyphosphoryl-2,2-dimethylpropyl)aminoxy)-propionic acid alkoxyamine (Bloc-Builder MA, BB) was kindly supplied by Arkema. 1,5,7-triazabicyclo[4.4.0]dec-5-ene (TBD, >98%) was purchased from TCI. Deuterated chloroform (CDCl₃) and tetrahydrofuran (d_8-THF) were purchased from Eurisotop. Tetrahydrofuran (THF, HPLC grade), methanol (MeOH, HPLC) and chloroform (CHCl₃, HPLC grade) were obtained from VWR Chemicals. Hydrochloric acid (HCl, 37%) was supplied by Carlo-Erba. 2.5% Active chlorine bleach solution was purchased from Leroy Merlin (France). Dibenzo[c,e]oxepane-5-thione (DOT),[39] gemcitabine-AMA-SG1 (Gem-AMA-SG1)[19] and 2-ethyl-sulfanylthiocarbonylsulfanylpropionic acid ethyl ester (ETSPE)[51] were prepared as reported elsewhere. Pressure tubes (Ace Glass 8648_164, 15 mL-capacity, fitted with a plunger valve and thermowell) were purchased from Sigma-Aldrich.

Analytical methods

Nuclear magnetic resonance (NMR) spectroscopy. NMR spectroscopy was performed in 5 mm diameter tubes in CDCl₃ or d_8-THF at 25 °C. ¹H NMR spectroscopy was performed on a Bruker Avance 300 spectrometer at 300 MHz with 350 scans. The chemical shift scale was calibrated based on the internal solvent signals ($\delta = 7.26$ ppm) for CDCl₃ and the TMS internal
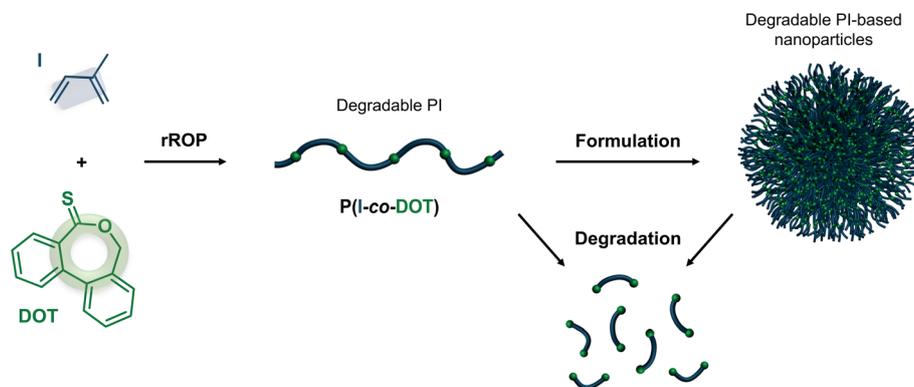

Fig. 1 Synthesis of degradable vinyl polymer nanoparticles via radical ring opening copolymerization (rROP) of dibenzo[c,e]oxepane-5-thione (DOT) and isoprene (I) in solution followed by nanoprecipitation.

standard ($\delta = 0$ ppm) for d_8-THF. ^{31}P NMR spectroscopy was conducted in CDCl$_3$ on a Bruker Avance 400 spectrometer operating at a frequency of 161.9 MHz with a 5 mm gradient BBFO probe (31P-109Ag/1H). The NMR spectra were recorded with proton decoupling (1D sequence with inverse gated ^{1}H-decoupling) with a spectral width of 32 467 Hz, an acquisition time of 1 s and a relaxation delay of 34 s. The chemical shift scale was calibrated based on added diethyl phosphite at $\delta = 7.1$ ppm.

Size exclusion chromatography (SEC). For kinetic monitoring, SEC on dry extracts was performed on a Tosoh EcoSEC HLC-8320 GPC with two columns from Agilent (PL-gel MIXED-D 300 × 7.5 mm, bead diameter 5 μm; linear part 400 to 400 000 g mol^{-1}). Analyses were performed at 35 °C in chloroform (HPLC grade) at a flowrate of 1 mL min^{-1} using toluene as a flowrate marker. A conventional calibration curve was constructed based on polystyrene (PS) standards (peak molar masses: $M_p = 575$–126 500 g mol^{-1}) from Polymer Laboratories. A PI calibration curve was constructed by converting the PS standard peak molecular weights, M_{PS}, to PI molecular weights, M_{PI}, using MarkHouwink–Sakurada (MHS) constants determined for both polymers in CCl$_4$ at 25 °C. For PI, the MHS constants used were $K_{PI} = 2.44 \times 10^{-4}$ and $\alpha_{PI} = 0.712$. For PS, $K_{PS} = 7.1 \times 10^{-4}$ and $\alpha_{PS} = 0.54$ ($M_W < 16 700$ g mol^{-1}) or $K_{PS} = 1.44 \times 10^{-4}$ and $\alpha_{PS} = 0.713$ ($M_W \geq 16 700$ g mol^{-1}).[52,53] This technique allowed M_n (the number-average molar mass), M_w (the weight-average molar mass), and M_w/M_n (the dispersity, Đ) to be determined.

For purified and degraded samples, SEC was performed at 30 °C with two columns from Agilent (PL-gel MIXED-D; 300 × 7.5 mm; bead diameter, 5 μm; linear part, 400–400 000 g mol^{-1}) and a differential refractive index detector (Spectrasystem RI-150 from Thermo Electron Corp.), using CHCl$_3$ as an eluent at a flowrate of 1 mL min^{-1} and toluene as a flowrate marker. A conventional calibration curve was constructed based on PS standards (peak molar masses: $M_p = 575$–126 500 g mol^{-1}) from Polymer Laboratories. A PI calibration curve was constructed in the same manner as described above. SEC of degraded copolymers was performed in the presence of 0.1% (v/v) of trifluoroacetic acid (TFA, 99%) in CHCl$_3$ (in both the mobile phase and the sample) to avoid the formation of aggregates and/or interaction with the columns and sulfhydryle or hydroxyl chain ends.

Dynamic light scattering (DLS) and zeta potential (ζ). Intensity-averaged nanoparticle diameter (D_z), polydispersity index (PDI) and zeta potential were measured by DLS with a nano ZS from Malvern (173° scattering angle) at a temperature of 25 °C. Nanoparticle dispersions were diluted in MilliQ water (dilution 1/10 (v/v)) prior to analysis. The surface charge of the nanoparticles was investigated by ζ-potential (mV) measurement at 25 °C after dilution (1/10 v/v) with 1 mM NaCl, using the Smoluchowski equation.

Cryogenic transmission electron microscopy (cryo-TEM). The morphologies of P(I-co-DOT) and PI nanoparticles were observed by cryo-TEM. 5 μL of the nanoparticle suspension was diluted at 1.2 mg mL^{-1} just prior analysis and deposited onto a Lacey Formvar/carbon 300 mesh copper grid (Ted Pella). The excess was manually blotted with a filter paper and the residual thin film was immediately frozen by plunging into liquid ethane and cooled down at liquid nitrogen temperature using a Leica EM-CPC cryoplunger. Observation was performed using a JEOL 2100HC microscope (JEOL Europe) or a JEOL 2200FS field emission microscope (JEOL USA) operating under an acceleration voltage of 200 kV in zero-loss mode (slit was 20 eV). High-magnification images (2k × 2k pixels) were recorded using a CCD camera (Gatan, Inc.) with Digital Micrograph software.

Synthetic procedures

Synthesis of poly(isoprene-co-dibenzo[c,e]oxepane-5-thione) (P(I-co-DOT), F0–F2) by free-radical polymerization in solution. In a typical procedure (**F1**, Table 1), I (4 mL, 2.73 g, 40 mmol), DOT (0.091 g, 0.404 mmol, $f_{DOT,0} = 0.01$), DCP (0.025 g,

Table 1 Experimental conditions for the synthesis of P(I-co-DOT) copolymers by rROP and their macromolecular characteristics

	Entry	$f_{DOT,0}$ (mol%)	t (h)	$DP_{n,th}$	Conv. I[a] (wt%)	$M_{n,th}$[b] (g mol^{-1})	M_n[c] (g mol^{-1})	M_w[c] (g mol^{-1})	Đ[c]	F_{DOT}[d] (mol%)
FRP	**F0**	0	30	—	37	—	7200	11 000	1.53	0
	F1	1	30	—	38	—	10 000	16 400	1.64	2.7
	F2	2	30	—	40	—	10 400	17 000	1.63	4.6
NMP	**N0**	0	48	100	33	2700	2400	2900	1.19	0
	N1	1	48	100	37	2900	3100	3900	1.25	2.7
	N2	2	48	100	40	3100	3300	4400	1.32	4.4
	N3	2	48	215	36	5700	5300	8200	1.54	5.3
	N4	2	48	435	21	6600	4800	7100	1.48	9.7
	N5[e]	2	16	100	17	1800	1800	2200	1.29	6.6
	N6	3	20	500	18	6500	7900	8400	1.07	6.1
	N7[e]	3	20	500	22	8100	9300	10 700	1.15	6.9
RAFT	**R0**	0	24	500	11	3900	3400	3900	1.16	0
	R1	2	24	500	10	3800	4500	6100	1.36	5.5
	R2	2	72	600	55	22 900	11 000	18 200	1.67	3.9

[a] Determined by gravimetry. [b] Determined according to: $M_{n,th} = M_{n,BB} + DP_{n,th} \times$ conv. MW$_I$. [c] Determined by SEC on precipitated samples. [d] Determined by ^{1}H NMR in d_8-THF of precipitated samples by integrating the 8H (Ar) of open DOT at 6.7–8 ppm and protons from PI (1H for the (1,4) conformation at 5–5.5 ppm, 1H for the (1,2) conformation at 5.5–5.9 ppm and 4.4–5 ppm combining 2H of (1,2) and 2H of (3,4) conformations). For **F1–F2** and **R1–R2**, the aromatic signal of DCP at 7.0–7.5 ppm was subtracted from the aromatic signal of DOT according to the DCP/PI ratio calculated on the **F0** and **R0** spectrum respectively. [e] The Gem-AMA-SG1 alkoxyamine was used instead of the BB alkoxyamine.

0.093 mmol) and dioxane (5 mL) were introduced in a pressure tube fitted with a plunger valve and thermowell. The solution was subjected to three cycles of freeze-thaw degassing, and then backfilled with argon. The tube was placed in an oil bath at 115 °C for 30 h at 300 rpm and then cooled down at room temperature. The I conversion was determined by gravimetry. The copolymer was purified by three successive precipitations in MeOH to remove unreacted DOT and dried under vacuum at room temperature. The resulting copolymer was analysed by ^{1}H NMR in d_8-THF and by SEC in CHCl$_3$.

The same procedure was adapted by varying the initial feed ratio of DOT ($f_{DOT,0}$) as follows: **F0** [I (4 mL, 2.73 g, 40 mmol) and DCP (0.025 g, 0.093 mmol) in 5 mL of dioxane] and **F2** [I (4 mL, 2.73 g, 40 mmol), DOT (0.185 g, 0.816 mmol, $f_{DOT,0}$ = 0.02) and DCP (0.025 g, 0.093 mmol) in 5 mL of dioxane].

The determination of the reactivity ratios was performed according to the following protocol. In a typical procedure, I (0.08 mL, 54 mg, 0.79 mmol), DOT (179 mg, 0.79 mmol, $f_{DOT,0}$ = 0.5), DCP (0.9 mg, 0.0036 mmol), anhydrous DMSO (61 mg, 0.79 mmol) used as the internal reference, and dioxane (7 mL) were introduced in a pressure tube fitted with a plunger valve and thermowell. The solution was subjected to three cycles of freeze-thaw degassing, and then backfilled with argon. The tube was placed in an oil bath at 115 °C for 1 h 30 and then cooled down at room temperature. The monomer conversions (kept at a low level; 34% maximum) were determined by ^{1}H NMR in CDCl$_3$ by integrating the signal at 6.4 ppm for I (dd, 1H), the signal at 8.2 ppm for DOT (d, 1H), and the signal of the internal reference at 2.6 ppm (d_6-DMSO, s, 6H). The copolymer was then purified by two successive precipitations in MeOH to remove unreacted DOT and dried under vacuum at room temperature. The resulting copolymer was analysed by ^{1}H NMR in d_8-THF to determine F_{DOT}. Different $f_{DOT,0}$ values were considered (0.1, 0.2, 0.3, 0.4, 0.5, 0.6, 0.7 and 0.9) by keeping a total monomer concentration of 1.13 M (Table S1†). Evolution of F_{DOT} with $f_{DOT,0}$ was then plotted, and the reactivity ratios were determined using nonlinear least-squares (NLLS) analysis performed with the CONTOUR software.[54]

Synthesis of P(I-*co*-DOT) (N0–N4 and N6) by NMP in solution. The experimental protocol was adapted from a previous report.[55] In a typical procedure (**N2**, Table 1), a mixture of I (6 mL, 4.086 g, 60 mmol), DOT (0.277 g, 1.22 mmol, 2 eq., $f_{DOT,0}$ = 0.02), BB (0.229 g, 0.60 mmol, 1 eq.) and dioxane (6 mL) was divided into 6 pressure tubes fitted with a plunger valve and thermowell. Each solution was subjected to three cycles of freeze-thaw degassing, and then backfilled with argon. The tubes were placed in an oil bath at 115 °C for 1, 3, 7, 16, 30 and 48 h, and then cooled down at room temperature. The I conversion was determined by gravimetry and the dry samples were analysed by SEC. The copolymer obtained at 48 h was purified by three successive precipitations in MeOH to remove unreacted DOT, dried under vacuum at room temperature and analysed by ^{1}H NMR in d_8-THF and by SEC in CHCl$_3$.

The same procedure was then adapted by varying $f_{DOT,0}$ and the targeted number-average degree of polymerization of I (DP$_{n,th}$) as follows: **N0** [I (6 mL, 4.086 g, 60 mmol, 100 eq.), BB (0.229 g, 0.60 mmol, 1 eq.) and dioxane (6 mL)]; **N1** [I (6 mL,

4.086 g, 60 mmol, 100 eq.), DOT (0.137 g, 0.61 mmol, 1.01 eq., $f_{DOT,0}$ = 0.01), BB (0.229 g, 0.60 mmol, 1 eq.) and dioxane (6 mL)]; **N3** [I (6 mL, 4.086 g, 60 mmol, 215 eq.), DOT (0.277 g, 1.22 mmol, 4.4 eq., $f_{DOT,0}$ = 0.02), BB (0.106 g, 0.279 mmol, 1 eq.) and dioxane (6 mL)]; **N4** [I (6 mL, 4.086 g, 60 mmol, 435 eq.), DOT (0.277 g, 1.22 mmol, 8.88 eq., $f_{DOT,0}$ = 0.02), BB (0.053 g, 0.138 mmol, 1 eq.) and dioxane (6 mL)] and **N6** [I (1.50 mL, 1.02 g, 15 mmol, 500 eq.), DOT (0.105 g, 0.46 mmol, 15.5 eq., $f_{DOT,0}$ = 0.03), BB (0.0114 g, 0.03 mmol, 1 eq.) and dioxane (1.50 mL)]. For **N3′** [I (6 mL, 4.086 g, 60 mmol, 215 eq.), DOT (0.277 g, 1.22 mmol, 4.4 eq., $f_{DOT,0}$ = 0.02), BB (0.106 g, 0.279 mmol, 1 eq.), dioxane (6 mL) and anhydrous DMSO (0.056 mL, 0.123 g, 1.5 mmol)], anhydrous DMSO was added as an internal reference to determine the DOT conversion by ^{1}H NMR in CDCl$_3$.

Synthesis of P(I-*co*-DOT) (R0–R2) by RAFT polymerization in solution. The experimental protocol was adapted from a previous report.[56] In a typical procedure (**R1**, Table 1), I (2.86 g, 42 mmol, 500 eq.), DOT (0.193 g, 0.85 mmol, 10.2 eq., $f_{DOT,0}$ = 0.02), ETSPE (0.02 g, 0.084 mmol, 1 eq.) and DCP (0.0045 g, 0.016 mmol, 0.2 eq.) were introduced in a pressure tube fitted with a plunger valve and thermowell. The solution was subjected to three cycles of freeze-thaw degassing, and then backfilled with argon. The tube was placed in an oil bath at 115 °C for 24 h and then cooled down at room temperature. The I conversion was determined by gravimetry. The copolymer was purified by three successive precipitations in MeOH to remove unreacted DOT and dried under vacuum at room temperature. The resulting copolymer was analysed by ^{1}H NMR in d_8-THF and by SEC in CHCl$_3$.

The same procedure was then adapted by varying $f_{DOT,0}$, DP$_{n,th}$ and reaction time as follows: **R0** [I (2.86 g, 42 mmol, 500 eq.), ETSPE (0.02 g, 0.084 mmol, 1 eq.) and DCP (0.0045 g, 0.016 mmol, 0.2 eq.)] and **R2** [I (1.47 g, 21.6 mmol, 600 eq.), DOT (0.099 g, 0.441 mmol, 12.25 eq., $f_{DOT,0}$ = 0.02), ETSPE (0.008 g, 0.036 mmol, 1 eq.) and DCP (0.0019 g, 0.007 mmol, 0.2 eq.) for 72 h].

Synthesis of gemcitabine-poly(isoprene-*co*-dibenzo[*c,e*] oxepane-5-thione) (Gem-P(I-*co*-DOT), N5 and N7) by NMP in solution. The experimental protocol was adapted from a previous report.[19] In a typical procedure (**N5**, Table 1), a solution of I (0.85 mL, 0.578 g, 85 mmol, 100 eq.), DOT (0.039 g, 0.17 mmol, 2.04 eq., $f_{DOT,0}$ = 0.02), and Gem-AMA-SG1 (0.052 g, 0.085 mmol, 1 eq.) was added into 0.85 mL of dioxane and introduced in a pressure tube fitted with a plunger valve and thermowell. The solution was subjected to three cycles of freeze-thaw degassing, and then backfilled with argon. The tube was placed in an oil bath at 115 °C for 16 h and then cooled down at room temperature. The I conversion was determined by gravimetry. The copolymer was purified by three successive precipitations in MeOH to remove unreacted DOT and dried under vacuum at room temperature. The resulting copolymer was analysed by ^{1}H NMR in CDCl$_3$ and by SEC in CHCl$_3$. The drug content in gemcitabine (Gem) was determined according to: %Gem = MW$_{Gem}$/$M_{n,Gem-PI}$ with MW$_{Gem}$ = 263.2 g mol^{-1}.

The same procedure was then adapted by targeting DP$_{n,th}$ = 500 as follows: **N7** [I (1.30 mL, 0.885 g, 13 mmol, 500 eq.)], DOT

(0.091 g, 0.40 mmol, 15 eq., $f_{DOT,0} = 0.03$), Gem-AMA-SG1 (0.016 g, 0.026 mmol, 1 eq.) and 1.30 mL of dioxane.

Nanoparticle preparation

Nanoparticles were prepared by the nanoprecipitation technique. Briefly, 10 mg of polymer **N0–N5** (Table 1) were dissolved in 2 mL of THF and added dropwise to 3 mL MilliQ water under stirring. THF was removed under vacuum to reach a final concentration of 3.3 mg mL^{-1}. For **N6**, 20 mg of polymer (Table 1) were dissolved in 8 mL of dioxane and added dropwise to 12 mL MilliQ water under stirring. Dioxane was removed under vacuum to reach a final concentration of 1.7 mg mL^{-1}. For **N7**, volumes of dioxane and water were divided by two to reach a final concentration of 3.3 mg mL^{-1}. Intensity-average diameter (D_z) and zeta potential measurements were carried out in triplicate.

Degradation procedures

Degradation of the copolymers by KOH. 10 mg of copolymer were solubilized in 0.5 mL of DCM prior to adding 0.5 mL of a 5 wt% aqueous solution of KOH in MeOH. The solution was stirred for 16 h at room temperature and dried under vacuum. HCl solution (1 M) was then added to the organic solution followed by extraction of the aqueous layer (three times). Solvent was removed under reduced pressure. The degradation products were analysed by SEC.

Degradation of the copolymers by isopropylamine. 10 mg of copolymer were solubilized in 1 mL of THF prior to adding 0.4 mL of isopropylamine. The solution was stirred for 16 h at room temperature. THF and isopropylamine were removed under vacuum. The degradation products were analysed by SEC.

Degradation of the copolymers by TBD. 10 mg of copolymer were solubilized in 0.5 mL of THF prior to adding 0.5 mL of a 5 wt% solution of TBD in THF. The solution was stirred for 16 h at room temperature and dried under vacuum. The organic solution was washed three times with HCl solution (1 M) to remove TBD and then dried under vacuum until constant weight. The degradation products were analysed by SEC.

Degradation of the nanoparticles by bleach solution. In a typical procedure, 1 mL of nanoparticle suspensions **N6** (Table 4, 1.7 mg mL^{-1}) and **N7** (Table 4, 3.3 mg mL^{-1}) was added to 2 mL of 2.5% active chlorine bleach solution. The solution was stirred for 12 days at room temperature. The product was extracted with 2 mL CHCl$_3$. The organic solvent was dried with MgSO$_4$, filtered, and evaporated under reduced pressure. The degradation products were analysed by SEC.

Degradation of the nanoparticles by cysteine and glutathione (GSH). Degradant solutions were prepared by dissolving cysteine or glutathione and tris(carboxyethyl phosphine) TCEP with a 10/1 thiol/TCEP molar ratio in PBS pH 7.4. The pH of solutions was adjusted by adding 0.5 M NaOH solution to 7.4 for cysteine solution and 7.2 for glutathione solution. PBS was added to adjust the concentration of thiol to 20 mM. 1 mL of **N6** (Table 4, 1.7 mg mL^{-1}) or 0.5 mL of **N7** (Table 4, 3.3 mg mL^{-1}) and 0.5 mL water were added to 1 mL thiol 20 mM solution resulting in 10 mM thiol solutions. The solutions were stirred at

37 °C for 15 days. The mixture was extracted with 2 mL CHCl$_3$. The organic solvent was dried with MgSO$_4$, filtered, and evaporated under reduced pressure. The degradation products were analysed by SEC.

In vitro cytotoxicity

Cell lines and cell culture. Human umbilical vein endothelial cells (HUVEC), mouse monocyte macrophage cells (J774.A1) and lung cancer cells (A549) were obtained from the American Type Culture Collection (Molsheim, France) and maintained as recommended. HUVEC cells were grown in Dulbecco's modified Eagle medium (DMEM) with high glucose supplemented with 10% fetal bovine serum (FBS), penicillin (100 U mL^{-1}) and streptomycin (100 U mL^{-1}). J774.A1 cells were grown in Roswell Park Memorial Institute medium (RPMI) 1640 supplemented with 10% FBS, penicillin (100 U mL^{-1}) and streptomycin (100 U mL^{-1}). A549 cells were cultured in Roswell Park Memorial Institute medium (RPMI) and supplemented with 10% FBS and penicillin (100 U mL^{-1}). Cells were maintained in a humid atmosphere at 37 °C with 5% CO$_2$.

Cytotoxicity assay (MTT). MTT [3-(4,5-dimethylthiazol-2-yl)-2,5-diphenyl tetrazolium bromide] was used to test the cytotoxicity of the different nanoparticles *via* cell viability measurement. Briefly, cells (5×10^3 per well) were seeded in 96-well plates. After a 24 h incubation, cells were exposed to a series of increasing concentrations of nanoparticles. After 72 h, 20 μL of MTT solution (5 mg mL^{-1} in PBS) was added to the medium in each well. The plates were incubated for 1 h at 37 °C and the medium was removed after centrifugation. 200 μL of DMSO were then added to each well to dissolve the precipitates. Absorbance was measured at 570 nm using a plate reader (Metertech Σ 960, Fisher Bioblock, Illkirch, France). The percentage of surviving cells was calculated as the absorbance ratio of treated to untreated cells. All experiments were set up in sextuplicate to determine means and SDs.

Cytotoxicity of the degradation products. The degraded copolymers by TBD were dissolved in CHCl$_3$ and filtered 3 times to remove the residual salts. They were dried under vacuum until constant weight. Due to the insolubility of the degradation products in water, they were dispersed in aqueous media as follows: For J774.A1 cells, the degradation products were dissolved in DMSO and added drop by drop to MilliQ water under stirring to reach a final concentration of 5 v% of DMSO. A control experiment with a 5 v% solution of DMSO in MilliQ water was performed on cells and no cytotoxicity was shown in the concentration range considered. For HUVEC cells, the degradation products were dissolved in THF and added dropwise to MilliQ water under stirring. THF was removed under vacuum.

Results and discussion

Synthesis of DOT-containing polyisoprene

Copolymerization of DOT with **I** was first investigated by free-radical copolymerization in dioxane at 115 °C (Fig. 2). Initial molar fractions in DOT ($f_{DOT,0}$) up to 2 mol% were considered
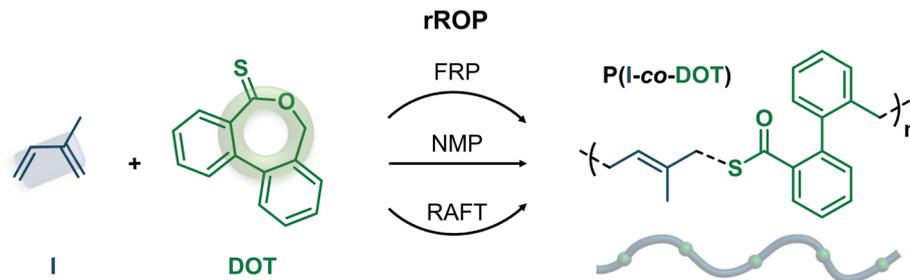
Fig. 2 Synthesis of poly(isoprene-*co*-dibenzo[*c*,*e*]oxepane-5-thione) (P(I-*co*-DOT)) copolymers by radical ring-opening copolymerization (rROP) of DOT and I in dioxane at 115 °C by: (a) free-radical polymerization (FRP); (b) nitroxide-mediated polymerization (NMP) and (c) reversible addition–fragmentation chain-transfer (RAFT) polymerization.

due its low solubility in dioxane. After 30 h of copolymerization, experiments **F1** ($f_{DOT,0} = 0.01$) and **F2** ($f_{DOT,0} = 0.02$) resulted in ~40% conversion of I and M_ns of ~10 000 g mol⁻¹ (Table 1).

Homopolymerization of I under identical polymerization conditions gave similar results (**F0**, Table 1), suggesting no retardation effect of DOT with I, in contrast to other vinyl monomers.[39,44] H^1 NMR spectroscopy was then performed on the purified (co)polymers, showing successful insertion of DOT units to an extent of $F_{DOT} = 2.7$ and 4.6 mol%, for experiments **F1** and **F2**, respectively (Fig. 3a and Table 1). Importantly, CKAs required a much higher initial feed ratio of 75 mol% to only incorporate 7 mol% of MDO in the PI backbone.[38] This was supported by theoretical DFT calculations that reported $r_{MDO} = 0.02$ and $r_I = 9.5$ (or $r_{BMDO} = 0.006$ and $r_I = 157$) at 70 °C for copolymerization between MDO (or BMDO) and I.[38] This therefore suggested a superior reactivity of DOT towards I compared to CKAs. Reactivity ratios of this copolymerization system were estimated using a NLLS method performed with the CONTOUR software,[54] giving $r_{DOT} = 4.29$ and $r_I = 0.14$ (the 95% joint confidence interval is given in Fig. S1†). This suggested a significant preferential incorporation of DOT over I and a high heterogeneity of the DOT fraction between chains if high conversion is reached (the latter expected from a FRP process). Similar trends, which can be explained by the structural similarity between DOT and RAFT agents, have been previously shown for the copolymerization of DOT with other vinyl monomers, such as *N,N*-dimethylacrylamide ($r_{DOT} = 1.89$ and $r_{DMAm} = 0.34$), *N*-2,3,4,5,6-pentafluorophenylmaleimide ($r_{DOT} = 0.198$ and $r_{PFPMI} = 0.0078$) and *N*-phenylmaleimide ($r_{DOT} = 0.348$ and $r_{PhMI} = 0.0136$).[41]

Copolymerizations *via* NMP and RAFT were then investigated to yield well-defined P(I-*co*-DOT) copolymers. NMP of I using BB as a SG1-based alkoxyamine was performed with $f_{DOT,0} = 1$ and 2 mol% in dioxane and with $DP_{n,th} = 100$ (**N0–N2**, Table 1). 30–40% conversions of I were obtained after 48 h, with M_n values in the 2400–3300 g mol⁻¹ range and low dispersities ($Đ = 1.19$–1.32), indicating a good control even in the presence of DOT. Interestingly, no noticeable retardation effect from DOT was obtained, despite the increasing initial molar fraction of DOT in the comonomer feed[39,44] (Fig. 3c). At $f_{DOT,0} = 2$ mol%, different $M_{n,th}$ were targeted by varying the $DP_{n,th}$ from 100 to 435 (**N2–N4**, Fig. 3c–e, Table 1). Interestingly, the

copolymerizations exhibited all the characteristics of a controlled system, as confirmed by: (i) the linear evolutions of the M_n values with I conversion, in pretty good agreement with the theoretical ones (Fig. 3d) and (ii) the low dispersities ($Đ < 1.2$) throughout the reactions (Fig. 3d and S2†). The final copolymers were then purified and analysed by ^1H NMR (Table 1, Fig. S3†), which successfully demonstrated insertion of open DOT units into the PI backbone at 4.4 and 5.3 mol% for **N2** and **N3**, respectively. The final amount of DOT in the copolymer was correlated to: (i) the initial stoichiometry, as the higher $f_{DOT,0}$, the higher the F_{DOT} (see **N1** and **N2**, Table 1) and (ii) the I conversion, as the lower the I conversion, the higher the F_{DOT}, in agreement with the reactivity ratios and thus the expected composition drift of P(I-*co*-DOT) copolymers (see **N2–N4**, Table 1). In order to gain further insight into this copolymerization system, the evolutions of the individual conversions of DOT and I, as well as F_{DOT} during the copolymerization were studied for **N3**. Note that **N3** was repeated in the presence of DMSO as the internal reference and noted as **N3′** (Fig. 3e and S4†). It appeared that DOT was indeed consumed faster than I, leading to 85% DOT conversion and 37% I conversion after 48 h. As expected, the evolution of F_{DOT} progressively decreased from 15.5 to 4.3 mol% after 48 h in agreement with a gradient composition.

N3′ and **N0** were also analysed by ^{31}P NMR to perform in-depth chain-end characterization and give crucial insights into the nature of the copolymer terminal sequences and the living chain fractions.[57] Interestingly, the phosphorus signals (24.4–24.6 ppm) from **N3′** and **N0** had the same shape and were characteristic of I-SG1 terminal sequences (Fig. S5†),[53] thus ruling out accumulation of DOT as the last monomer unit and supporting its faster incorporation in the copolymer compared to I. By integrating these phosphorus signals and that of diethyl phosphite (7.1 ppm) used as an internal standard, the living-ness of both (co)polymers was estimated to be ~50%.

P(I-*co*-DOT) copolymers were also synthesized by RAFT polymerization using ETSPE as a RAFT agent[56] and DCP as a source of radicals. After 24 h with $f_{DOT,0} = 0.02$, 10% of I conversion was achieved giving $M_n = 4500$ g mol⁻¹ and $Đ = 1.36$ (**R1**, Table 1). The absence of DOT under the same conditions (**R0**, Table 1) led to very similar macromolecular characteristics, despite obtaining a lower dispersity ($Đ = 1.16$). To obtain higher
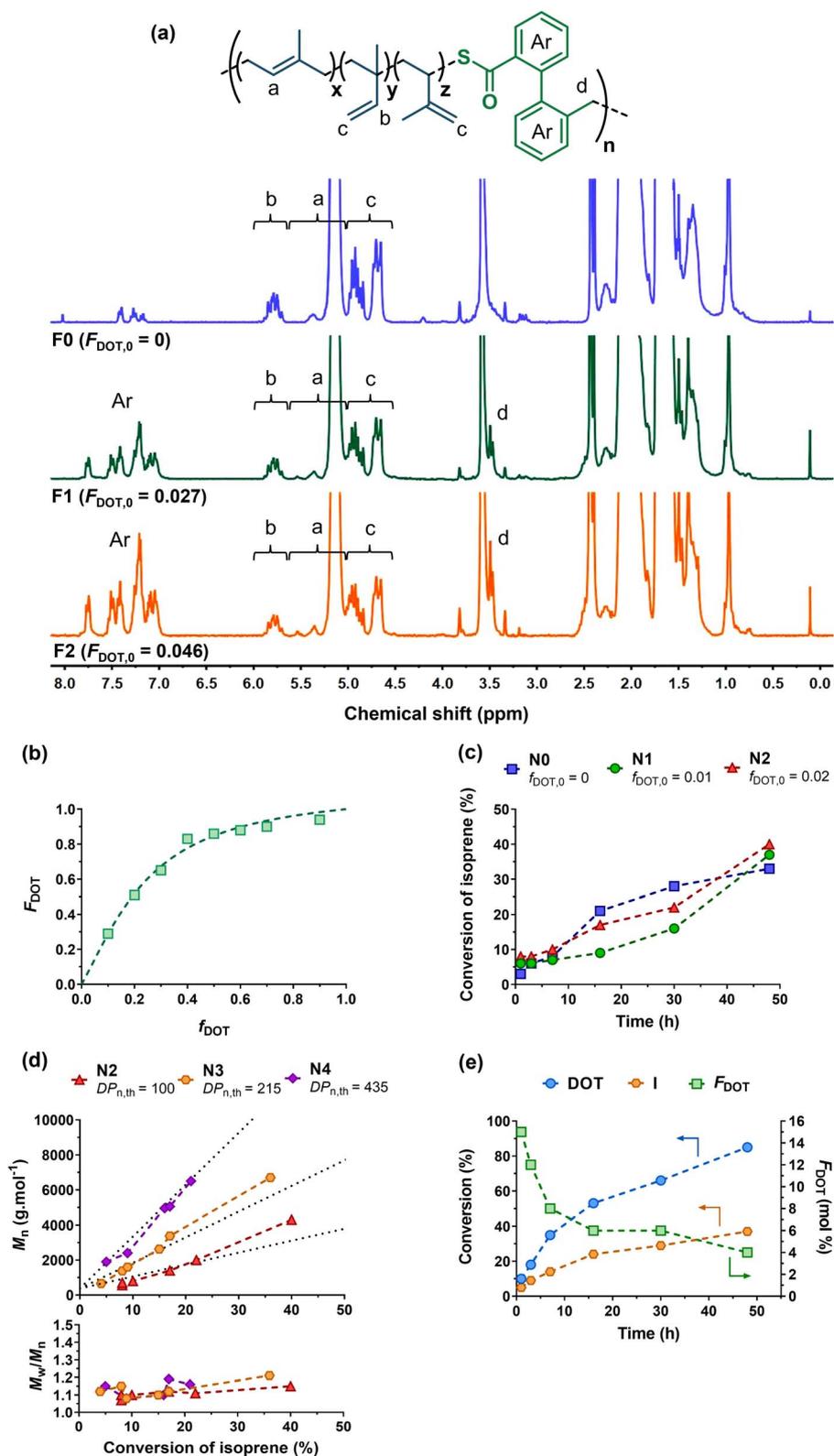
Fig. 3 (a) ^{1}H NMR spectrum (300 MHz, d_8-THF) in the 0–8 ppm region of P(I-*co*-DOT) copolymers **F0**, **F1** and **F2** (Table 1). (b) Evolution of molar DOT content in copolymers with molar DOT in the monomer feed with nonlinear least-squares fitted curves with $r_{DOT} = 4.29$ and $r_I = 0.14$. (c) Evolution of I conversion *vs.* time as a function of $f_{DOT,0}$ (**N0**, **N1** and **N2**, Table 1). (d) Evolution of M_n and Đ *vs.* I conversion as a function of $DP_{n,th}$ (**N2**, **N3** and **N4**, Table 1). (e) Evolution of I conversion, DOT conversion and average molar fraction of DOT (F_{DOT}) in the copolymer *vs.* time (**N3′**).

Table 2   Macromolecular characteristics of P(I-co-DOT) copolymers obtained by rROP before and after degradation

Entry	M_n (g mol^{-1})	M_w (g mol^{-1})	$Đ^a$	F_{DOT}^b (mol%)	$M_{n,deg,th}^c$ (g mol^{-1})	Degradation by KOH^d			Degradation by isopropylamine^e			Degradation by TBD^f		
						$M_{n,deg,KOH}$ (g mol^{-1}) (% M_n loss)	$M_{w,deg,KOH}$ (g mol^{-1}) (% M_w loss)	$Đ$	$M_{n,deg,isoprop}$ (g mol^{-1}) (% M_n loss)	$M_{w,deg,\,isoprop}$ (g mol^{-1}) (% M_w loss)	$Đ$	$M_{n,deg,TBD}$ (g mol^{-1}) (% M_n loss)	$M_{w,deg,TBD}$ (g mol^{-1}) (% M_w loss)	$Đ$
FRP														
F0	7200	11 000	1.53	0	7200	7200 (0)	11 000 (0)	1.52	7200 (0)	10 900 (−1)	1.52	7200 (0)	10 900 (−1)	1.51
F1	10 000	16 400	1.64	2.7	2700	5300 (−47)	10 800 (−34)	2.04	9600 (−4)	14 400 (−12)	1.50	2700 (−73)	4800 (−70)	1.76
F2	10 400	17 000	1.63	4.6	1600	4100 (−61)	8100 (−52)	1.98	9600 (−8)	15 600 (−8)	1.63	1700 (−84)	3200 (−81)	1.88
NMP														
N0	2400	2900	1.19	0	2400	2400 (0)	2900 (0)	1.20	2400 (0)	2900 (0)	1.19	2400 (0)	2900 (0)	1.20
N1	3100	3900	1.25	2.7	2700	1600 (−48)	2700 (−30)	1.69	3100 (0)	3900 (0)	1.26	1400 (−55)	2400 (−38)	1.71
N2	3300	4400	1.32	4.4	1700	1600 (−52)	2800 (−36)	1.73	3300 (0)	4400 (0)	1.35	1300 (−61)	2200 (−50)	1.66
N3	5300	8200	1.54	5.3	1400	1700 (−68)	2900 (−64)	1.73	5200 (−2)	7600 (−7)	1.47	1100 (−80)	2300 (−72)	2.10
N4	4800	7100	1.48	9.7	900	1000 (−79)	1600 (−77)	1.63	4700 (−3)	6700 (−6)	1.43	800 (−83)	1700 (−76)	2.10
N5^g	1800	2200	1.29	6.6	1200	—	—	—	—	—	—	700 (−61)	1000 (−55)	1.55
N6^g	7900	8400	1.07	6.1	1300	1700 (−78)	2640 (−68)	1.55	—	—	—	—	—	—
N7^g	9300	10 700	1.15	6.9	1150	2100 (−71)	4650 (−56)	2.22	—	—	—	—	—	—
RAFT														
R0	3400	3900	1.16	0	3400	3400 (0)	4300 (0)	1.26	—	—	—	3400 (0)	4400 (0)	1.28
R1	4500	6100	1.36	5.5	1400	1300 (−71)	3500 (−43)	2.63	—	—	—	900 (−80)	1800 (−70)	1.93
R2	11 000	18 200	1.67	3.9	1900	3300 (−70)	7600 (−58)	2.30	—	—	—	2300 (−79)	4300 (−76)	1.86

^{a} Determined by SEC on precipitated samples. ^{b} Determined by ^{1}H NMR in d_8-THF of precipitated samples by integrating the 8H (Ar) of open DOT at 6.7–8 ppm and protons from PI (1H for the (1,4) conformation at 5–5.5 ppm, 1H for the (1,2) conformation at 5.5–5.9 ppm and 4.4–5 ppm combining 2H of (1,2) and 2H of (3,4) conformations). For **F1**–**F2** and **R1**–**R2**, the aromatic signal of DCP at 7.0–7.5 ppm was subtracted from the aromatic signal of DOT according to the DCP/PI ratio calculated on the **F0** and **R0** spectrum respectively. ^{c} Determined according to: $M_{n,deg,th} = [[(1 - F_{DOT})/F_{DOT}) \times MW_I] + MW_{DOT}$. ^{d} Determined by SEC after degradation by KOH for 16 h. ^{e} Determined by SEC after degradation by isopropylamine for 16 h. ^{f} Determined by SEC after degradation by TBD for 16 h. % M_n loss is calculated according to: % M_n loss $= [(M_n - M_{n,\,deg})/M_n] \times 100$. ^{g} The Gem-AMA-SG1 alkoxyamine was used instead of the BB alkoxyamine.

molecular weights, the copolymerization reaction was then carried out for 72 h with $DP_{n,th} = 600$ (**R2**, Table 1) instead of 500. This time, 55% conversion was obtained as well as $M_n = 11\,000$ g mol^{-1} with however a higher dispersity ($Đ = 1.67$). The DOT contents in the P(I-co-DOT) copolymers were determined to be 5.5 and 3.9 mol% for **R1** and **R2**, respectively (Table 1 and Fig. S6†), which is also in line with the faster incorporation of DOT compared to I. Therefore, these results confirmed the ability of DOT to be inserted into the PI backbone by FRP, NMP and RAFT polymerization mechanisms.

Interestingly, the values of F_{DOT} vs. conversion for **F2**, **N2–N5**, **N3'** and **R1–R2** are in fairly good agreement with the theoretical evolution of F_{DOT} vs. conversion plotted using a PREDICI numerical simulation[58] that predicts the compositional drift occurring during the copolymerization between vinyl and cyclic monomers, with r_{DOT}, r_I and $f_{DOT,0}$ as the input parameters (Fig. S7†). This observation therefore validates the values of the reactivity ratios that we determined. It is also important to note that the copolymerization behaviour is dramatically different when the theoretical evolution of F_{MDO} vs. conversion is plotted using the corresponding reactivity ratios[38] and the same $f_{MDO,0}$ value as for DOT. Indeed, F_{MDO} values stay below 0.003 regardless of conversion, in contrast to F_{DOT} values that range from 0.12 to 0.02 with conversion. This result highlights the strong added value of DOT over CKA in incorporating weak bonds into polyisoprene chains.

Degradation of P(I-co-DOT) copolymers

Degradation of the copolymers was then performed to confirm the successful insertion of thioester groups. Different degradation conditions were used (e.g., KOH, TBD and isopropylamine)[39–44] to investigate hydrolysis and aminolysis as

two distinct degradation modalities (in addition to physiological[48] and oxidative[59] degradations of thioester-containing copolymers). In general, whatever the polymerization methods used to generate the copolymers, significant degradation was observed after their treatment with either KOH or TBD for 16 h (Table 2, Fig. 4, S8 and S9†). The decrease in M_n and M_w ranged from −47 to −79% with KOH and from −55 to −84% with TBD (Table 2). Conversely, the M_n of PI homopolymers (**F0**, **N0** and **R0**) after degradation under the same conditions stayed constant (Fig. S8–S10† and Table 2). The degradation was also in agreement with the DOT content as increasing $F_{DOT,0}$ from 0.027 (**F1**, Table 2) up to 0.046 (**F2**, Table 2) led to a higher decrease in M_n and M_w in the presence of TBD or KOH compared to **F1**. A similar trend was observed for copolymers obtained by NMP (**N1–N4**, Table 2). In addition, $M_{n,deg}$ values were in fairly good agreement with theoretical M_ns values of the copolymers after degradation ($M_{n,deg,th}$, Table 2). However, no degradation was shown in the presence of isopropylamine, which could be correlated to the strong hydrophobicity of PI, similar to that observed with styrene.[42,44]

Application to nanoparticles and polymer prodrug nanoparticles

Polymer nanoparticles for drug delivery purposes are usually obtained by formulation of preformed polymers such as aliphatic polyesters, poly(alkyl cyanoacrylate), etc.[60–64] These polymers, which are few in number, are chosen because of their biocompatibility and biodegradability compared to non-degradable materials, which can accumulate in the body and induce prohibitive side effects. In order to diversify the range of polymers suitable for biomedical applications, the design of (bio)degradable vinyl polymers is currently of great interest.[1]
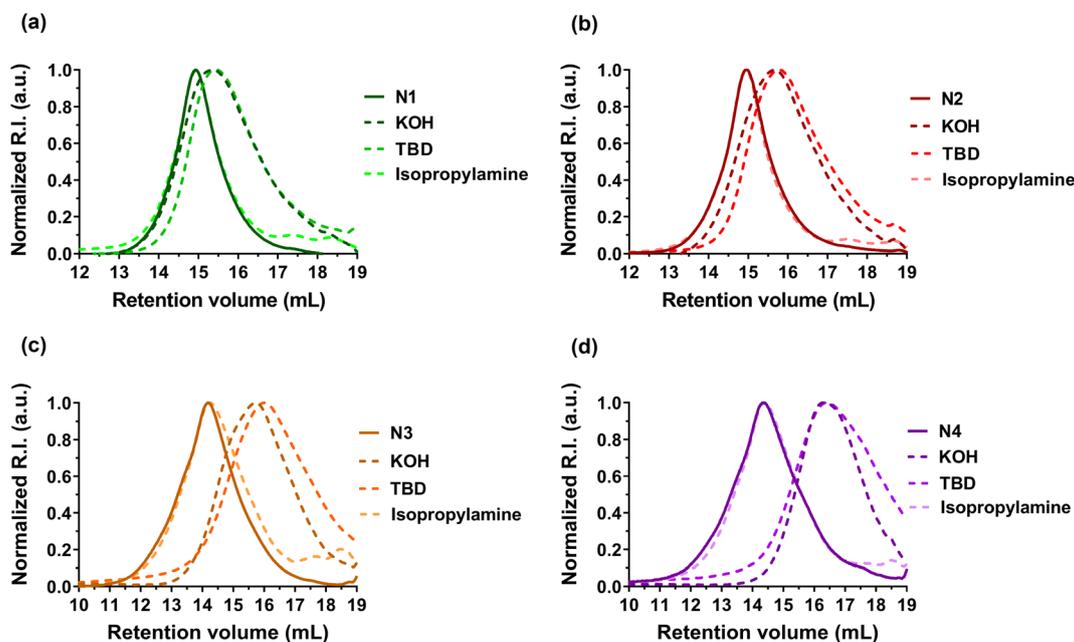

Fig. 4 Evolution of the SEC chromatograms of P(I-co-DOT) copolymers: (a) **N1**, (b) **N2**, (c) **N3**, and (d) **N4**, after degradation under basic (KOH or TBD) or aminolytic (isopropylamine) conditions.

Table 3 Colloidal and macromolecular characteristics of P(I-*co*-DOT) nanoparticles obtained by nanoprecipitation before and after degradation by TBD

Entry	$D_z{}^a$ (nm)	PDI^a	ζ (mV)	% M_n loss, $_{deg.TBD}{}^b$	% M_w loss, $_{deg.TBD}{}^b$	$Đ^b$
N0	150	0.09	−56	0	−3	1.17
N1	140	0.15	−27	−45	−30	1.58
N2	145	0.10	−50	−50	−26	2.30
N3	130	0.07	−46	−56	−48	2.05
N4	105	0.09	−27	−59	−39	2.24

^{a} Determined by DLS. ^{b} Determined by SEC after degradation of the nanoparticles in water with TBD for 48 h.

We illustrated the potential of the I/DOT copolymerization system for drug delivery purposes by first investigating the formulation of P(I-*co*-DOT) copolymers into nanoparticles (**N0**–**N4**, Table 3). Narrowly dispersed nanoparticles were successfully formed by nanoprecipitation, exhibiting an average diameter between 105 and 150 nm (Table 3 and Fig. S11†). The nanoparticle diameters also tended to decrease with the increase of the copolymer chain length, in agreement with previous data on PI nanoparticles.[19] This appeared to be attributed to an increase in hydrophobic interactions between PI chains as they lengthen, making the core of the nanoparticles more compact. All nanoparticles also exhibited strongly negative zeta potentials (Table 3), suggesting efficient electrostatic stabilisation, which was confirmed by their remarkable long-term colloidal stability up to one month (Table 3 and Fig. 5a, S12†). Cryo-TEM analysis also revealed the formation of nanoparticles with spherical morphologies (Fig. 5b). Overall,

insertion of thioester units in the PI backbone did not impact the colloidal characteristics (size, stability and morphology) of the nanoparticles compared to their non-degradable PI counterparts.[19]

Direct degradation of the nanoparticles was then attempted in the presence of TBD for 48 h at room temperature. Despite the strong hydrophobicity of the copolymer that may prevent efficient access of TBD to the hydrophobic core of nanoparticles, the decrease in M_n and M_w reached 40–59% and 26–48%, respectively (**N1**–**N4**, Table 3). The higher the F_{DOT}, the greater the degradation, even if this trend was less pronounced than that for the copolymers, probably for reasons of accessibility to the thioester group in the nanoparticulate state. However, longer degradation times and/or higher concentrations of TBD may have certainly enhanced the degradation of the nanoparticles.
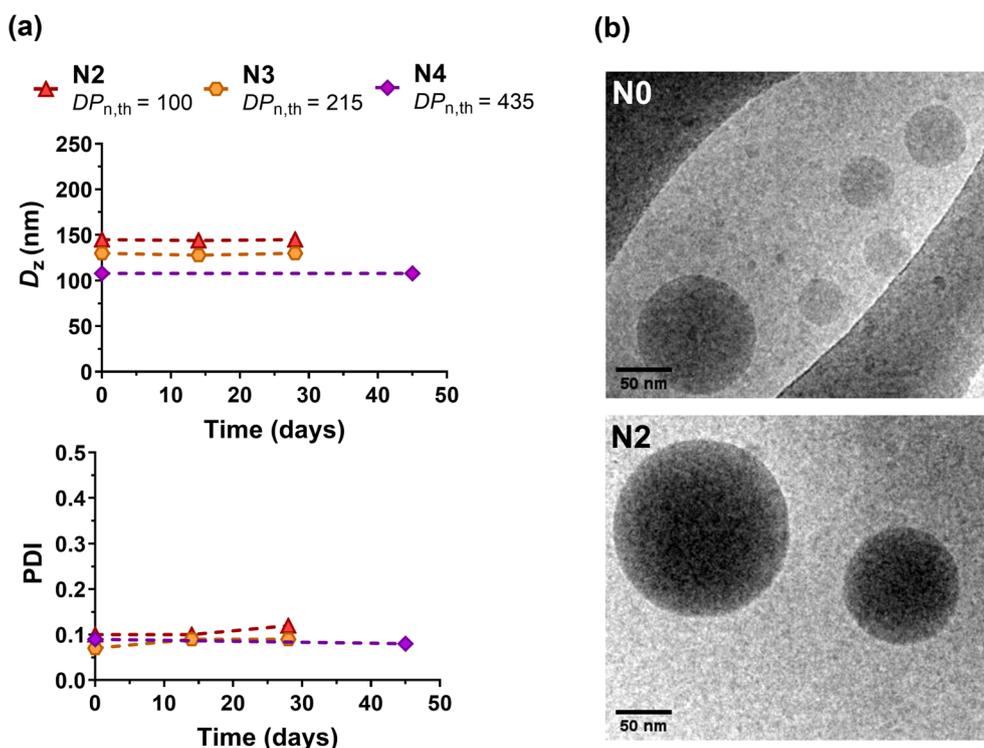
Fig. 5 (a) Evolution of the intensity-average diameter (D_z) and polydispersity index (PDI) with time measured by DLS of P(I-*co*-DOT) nanoparticles (**N2**, **N3** and **N4**, Table 3). (b) Representative cryo-TEM images of nanoparticles **N0** and **N2**.
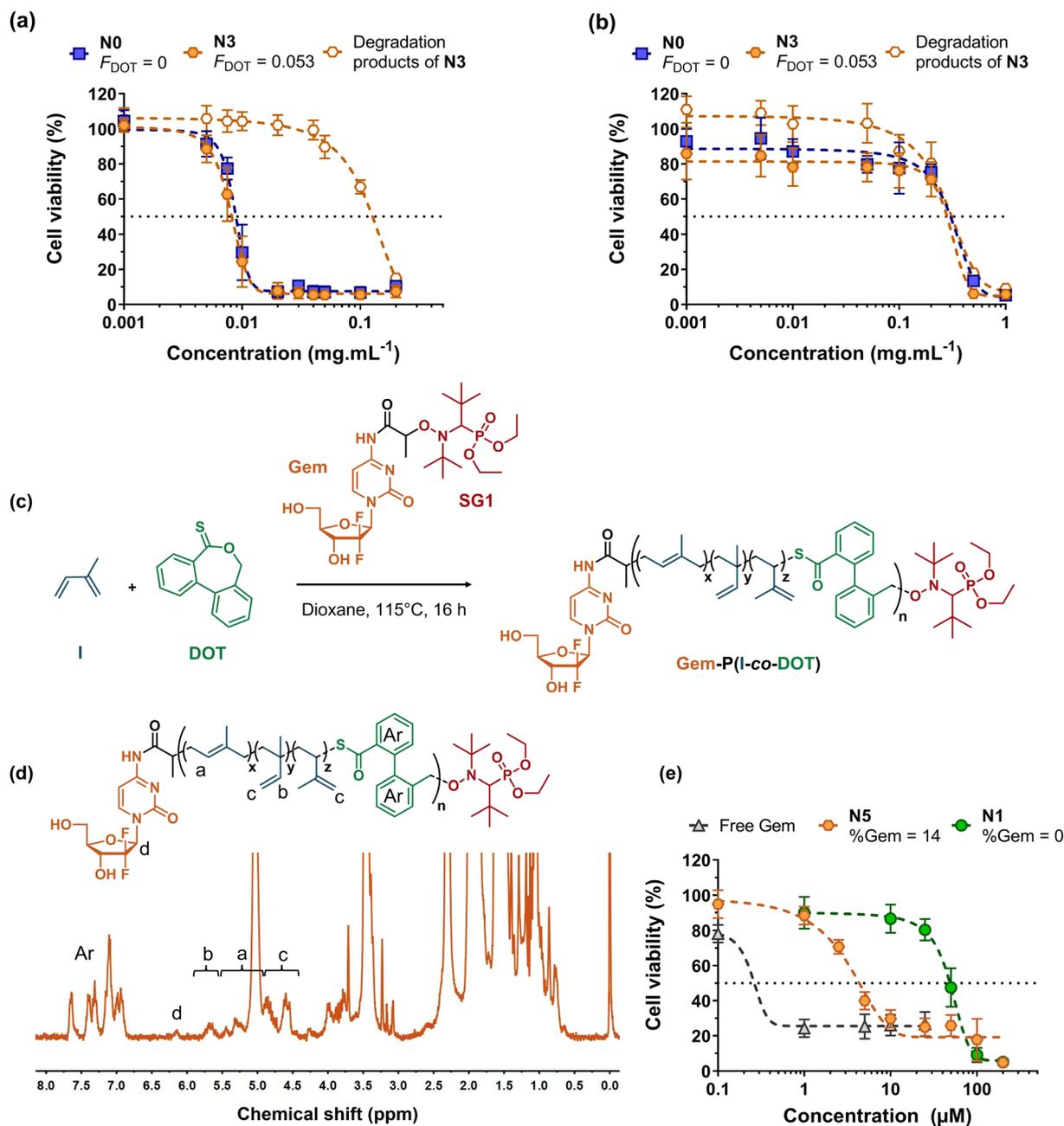
Fig. 6 Cell viability of: (a) murine macrophage (J774.A1) and (b) human endothelial cell (HUVEC) lines as a function of the concentration of nanoparticles **N3** and **N0** (Table 3) and of **N3** degradation products. (c) Synthesis of the Gem-P(I-*co*-DOT) polymer prodrug by radical ring-opening polymerization (rROP) of dibenzo[*c,e*]oxepane-5-thione (DOT) and isoprene (I) *via* nitroxide-mediated polymerization using a gemcitabine-functionalized macroalcoxyamine based on the nitroxide SG1 (Gem-AMA-SG1). (d) ^{1}H NMR spectrum (300 MHz, d_8-THF) in the 0−8 ppm region of the Gem-P(I-*co*-DOT) polymer prodrug **N5** (Table 1). (e) Cell viability of the lung cancer cell line (A549) as a function of the concentration of Gem-P(I-*co*-DOT) nanoparticles (**N5**, Table 1), P(I-*co*-DOT) nanoparticles (**N1**, Table 1) and free gemcitabine.

Cell viability experiments were then performed on two different healthy cell lines (J774.A1 and HUVEC), during which P(I-*co*-DOT) nanoparticles or the degradation products of the corresponding copolymers were evaluated (Fig. 6a and b). Half-maximal inhibitory concentrations (IC$_{50}$) of cell proliferation of 7.9 μg mL^{-1} and 0.31 mg mL^{-1} were obtained for J774.A1 and HUVEC cells, respectively. These values are identical to the IC$_{50}$ values obtained for PI nanoparticles (Fig. 6a and b),

demonstrating the absence of the cytotoxicity effect from DOT units. Moreover, the degradation products exhibited similar IC$_{50}$ values compared to the nanoparticles for HUVEC cells and much higher IC$_{50}$ values on J774.A1 cells (0.11 mg mL^{-1}). These results are very encouraging and let envision the use of P(I-*co*-DOT) as a carrier material for the design of degradable polymer nanoparticles for drug delivery.

Of the many polymer-based drug delivery systems developed to date, polymer-drug nanocarriers, in which the drug is covalently bound to the polymer, are the most promising because they circumvent the limitations associated with physical encapsulation of drugs (*e.g.*, burst release, poor drug loading, *etc.*).[65–68] While grafting drugs to a preformed polymer is the most popular strategy to produce polymer prodrugs, the "drug-initiated" method,[69] which consists in growing a polymer from a drug to obtain one drug molecule at the extremity of a well-defined polymer chain, has recently received increasing attention as an easy and scalable route to yield high drug loading, surfactant-free, vinyl polymer prodrug nanoparticles.[17,19,21,22,70–72] For instance, this has been applied to the synthesis of the Gem-polyisoprene prodrug by NMP, whose nanoparticles exhibited *in vitro* and *in vivo* anticancer activities on different cancer cell lines. However, they were not degradable, which may severely limit their development because of potential accumulation in the body and harmful side effects. Herein, we propose to apply the I/DOT copolymerization system to the synthesis of degradable Gem-P(I-*co*-DOT) prodrug nanoparticles (Fig. 6c). To install a Gem moiety at the α-position of P(I-*co*-DOT) copolymer chains, the copolymerization of I and DOT ($f_{DOT,0} = 0.02$) was initiated by the Gem-AMA-SG1 alkoxyamine. Gem-AMA-SG1 was obtained by coupling unprotected Gem to the AMA-SG1 alkoxyamine, resulting in an amide bond that can be selectively cleaved by cathepsin B, whose overexpression is correlated with invasive and metastatic cancers.[73,74] After 16 h (11% conv. in I), this yielded Gem-P(I-*co*-DOT) copolymers with $M_n = 1800$ g mol^{-1} and $Đ = 1.29$ (**N5**, Table 1). ^{1}H NMR analysis of **N5** confirmed the synthesis of the expected structure (Fig. 6d), particularly *via* the presence of Gem (peak d) and the characteristic proton signals of the PI

backbone, and gave $M_{n,NMR} = 2400$ g mol^{-1} (by integrating peak *a* from PI and peak d from Gem, Fig. 6d) in rather good agreement with the $M_{n,SEC}$ value (Table 1). Targeting such a low M_n allowed the prodrug to exhibit a Gem loading as high as 14 wt% with a F_{DOT} value of 6.6 mol% (Fig. 6d and Table 1). TBD-assisted degradation of Gem-P(I-*co*-DOT) prodrug **N5** led to a decrease in M_n and M_w of 61% and 55%, respectively (very close to the theoretical degradation), thus confirming the presence of thioester groups in the PI backbone and their successful cleavage (Table 2 and Fig. S13†). After nanoprecipitation, narrowly dispersed nanoparticles were obtained with $D_z = 140$ nm and a low PDI (0.11). They also showed a greater negative zeta potential value (-68 mV) than their drug-free counterparts (Table 3), suggesting the (partial) presence of Gem moieties at the surface nanoparticle surface, in agreement with molecular modelling experiments[75] for polymer prodrugs obtained by the "drug-initiated" method.

Gem-P(I-*co*-DOT) prodrug nanoparticles were then tested for their *in vitro* cytotoxicity on human lung carcinoma (A549) cells. Whereas drug-free P(I-*co*-DOT) nanoparticles gave an IC$_{50}$ of 49 µM, the prodrug nanoparticles led to a 35-fold-decrease in IC$_{50}$ (1.4 µM) (Fig. 6e). This demonstrates the cytotoxic activity of Gem-P(I-*co*-DOT) prodrug nanoparticles. As expected, free Gem exhibited a much greater cytotoxicity (IC$_{50}$ = 0.25 µM), since the free drug is immediately active whereas a prodrug must release the drug for it to be active. However, Gem is known to be quickly deaminated by deoxycytidine deaminase,[76] thus preventing its direct administration *in vivo* and requiring the use of protecting nanocarriers/prodrugs.

After establishing the degradation of P(I-*co*-DOT) nanoparticles by TBD (Table 3), the final step of this work was to study their degradation under physiological conditions, which
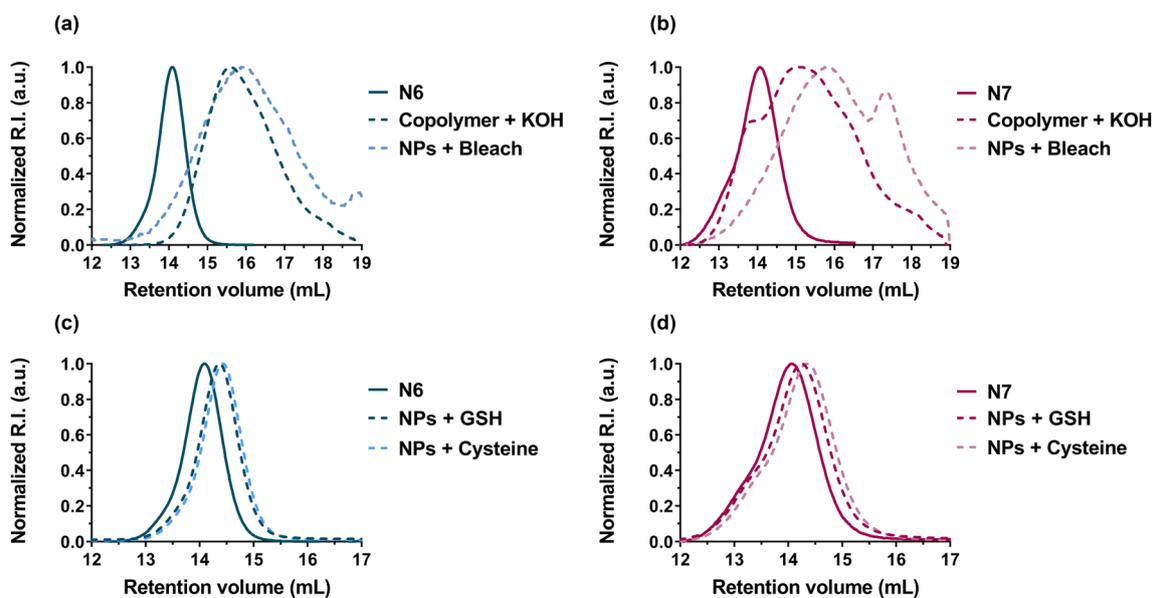

Fig. 7 SEC chromatograms of: (a) P(I-*co*-DOT) polymer (**N6**, see Table 1) and (b) Gem-P(I-*co*-DOT) prodrug (**N7**, see Table 1) after degradation in the presence of KOH (5 wt%, 20 °C) on the polymer and chlorine bleach solution (2.5%, 20 °C) on the nanoparticles. SEC chromatograms of: (c) P(I-*co*-DOT) polymer (**N6**, see Table 1) and (d) Gem-P(I-*co*-DOT) prodrug (**N7**, see Table 1) after degradation in the presence of cysteine (pH 7.4, PBS, 37 °C) and glutathione (pH 7.2, PBS, 37 °C) on the nanoparticles.

Table 4 Colloidal and macromolecular characteristics of P(I-co-DOT) **N6** and Gem-P(I-co-DOT) **N7** nanoparticles obtained by nano-precipitation before and after degradation by bleach solution, cysteine or glutathione (GSH)

Entry	$D_z{}^a$ (nm)	PDI^a	ζ (mV)	Degradation by bleach solution[b]			Degradation by cysteine[c]			Degradation by GSH[d]		
				$M_{n,deg.bleach}$ (g mol^{-1}) (% M_n loss)	$M_{w,deg.bleach}$ (g mol^{-1}) (% M_w loss)	Đ	$M_{n,deg.cysteine}$ (g mol^{-1}) (% M_n loss)	$M_{w,deg.cysteine}$ (g mol^{-1}) (% M_w loss)	Đ	$M_{n,deg.GSH}$ (g mol^{-1}) (% M_n loss)	$M_{w,deg.GSH}$ (g mol^{-1}) (% M_w loss)	Đ
N6	185	0.08	−37	1800 (−77)	2900 (−65)	1.60	6300 (−20)	6950 (−17)	1.10	6500 (−18)	7200 (−14)	1.11
N7[e]	130	0.08	−41	2600 (−65)	3900 (−63)	1.47	6600 (−19)	8300 (−11)	1.25	7100 (−12)	8600 (−8)	1.21

[a] Determined by DLS. [b] Determined by SEC after degradation of the nanoparticles by 2.5% active chlorine bleach solution during 12 days at 20 °C. [c] Determined by SEC after degradation of the nanoparticles in the presence of cysteine in PBS pH 7.4 during 15 days at 37 °C. [d] Determined by SEC after degradation of the nanoparticles in the presence of GSH in PBS pH 7.2 during 15 days at 37 °C. [e] The Gem-AMA-SG1 alkoxyamine was used instead of BB alkoxyamine.

is a key issue when developing biodegradable drug delivery systems. To this end, two model copolymers were synthesized: P(I-co-DOT) **N6** (M_n = 7900 g mol^{-1} and F_{DOT} = 6.1 mol%) and Gem-P(I-co-DOT) **N7** (M_n = 9300 g mol^{-1} and F_{DOT} = 6.9 mol%). They were then formulated by nanoprecipitation into nanoparticles (Table 4) exhibiting high colloidal stability for up to at least 14 days (**N6**: D_z = 185 nm, PDI = 0.08 and **N7**: D_z = 130 nm, PDI = 0.08).

Spurred by the physiological thiolytic degradability of DOT-containing copolymers,[48] the nanoparticles were subjected to degradation in the presence of: (i) chlorine bleach solution (2.5% sodium hypochlorite, 20 °C), which mimics both oxidative and base-catalysed hydrolysis due to the oxidative and alkaline nature of bleach, respectively[59] and (ii) cysteine (10 mM, pH 7.4, PBS, 37 °C) or glutathione (10 mM, pH 7.2, PBS, 37 °C), which mimic reductive degradations under physiological conditions. Note that using degradation under alkaline conditions is a routine procedure in rROP, which is used to anticipate and predict the degradation of rROP-derived copolymers in the long run. For instance, this is usually performed with ester-containing copolymers obtained by rROP of CKA and vinyl monomers.[77–80]

Degradation of nanoparticles **N6** and **N7** under oxidative/alkaline conditions (Fig. 7a,b and Table 4) resulted in a significant decrease in M_n and M_w (~60–80% after 12 days), which was similar to the degradation of the corresponding copolymers under alkaline conditions (KOH 5 wt%, see Table 2). More importantly, degradation of nanoparticles **N6** and **N7** under physiological reductive conditions successfully occurred (Table 4). As expected, the degradation kinetics were slower (~10–20% decrease in M_n or M_w after 15 days) than under oxidative/alkaline conditions, but significantly faster than the hydrolytic degradation under physiological conditions of most CKA-containing copolymers, which typically degrade over several months and even a year.[81–83] Overall, these results confirmed that P(I-co-DOT) and Gem-P(I-co-DOT) nanoparticles could be degraded under physiological conditions.

Conclusion

We successfully synthesized a small library of thionolactone-containing polyisoprene by radical ring-opening

copolymerization of isoprene and DOT, under either FRP, NMP and RAFT polymerization conditions. The resulting P(I-co-DOT) copolymers exhibited predictable M_n, low dispersity and tuneable DOT contents (2.7–9.7 mol%) simply by adjusting the copolymerization conditions. The copolymers were significantly degraded under basic conditions, which confirmed the successful insertion of open DOT units in the PI chains. Cytocompatible, narrowly dispersed, surfactant-free nanoparticles were also prepared by nanoprecipitation of P(I-co-DOT) copolymers, with average diameters suitable for drug delivery purposes. As a proof of concept, well-defined Gem-P(I-co-DOT) polymer prodrug nanoparticles were produced, which exhibited significant cytotoxicity on A549 cancer cells, as well as degradation under oxidative/alkaline conditions and reductive physiological conditions. In conclusion, DOT represents a promising monomer that can easily introduce labile thioester groups into PI chains via rROP and advantageously broaden the range of degradable vinyl materials, not only in nanomedicine but also for other applications involving PI.

Data availability

The authors declare that all data supporting the findings of this study are available within the article and ESI,† and raw data files are available from the corresponding author upon request.

Author contributions

M. L.: investigation, writing – original draft, data curation, visualization. C. Z.: investigation, data curation. T. P.: investigation, data curation. D. L.: investigation, data curation. J. M.: investigation, data curation. Y. G.: formal analysis, software, writing – review & editing. J. N.: conceptualization, visualization, writing – review & editing, funding acquisition, supervision, resources.

Conflicts of interest

There are no conflicts to declare.

Acknowledgements

References

1 V. Delplace and J. Nicolas, *Nat. Chem.*, 2015, **7**, 771–784.
2 R. Wei, T. Tiso, J. Bertling, K. O'Connor, L. M. Blank and U. T. Bornscheuer, *Nat. Catal.*, 2020, **3**, 867–871.
3 A. Rahimi and J. M. García, *Nat. Rev. Chem.*, 2017, **1**, 0046.
4 The future of plastic, *Nat. Commun.*, 2018, **9**, 2157, https://doi.org/10.1038/s41467-018-04565-2.
5 T. Pesenti and J. Nicolas, *ACS Macro Lett.*, 2020, **9**, 1812–1835.
6 A. Tardy, J. Nicolas, D. Gigmes, C. Lefay and Y. Guillaneuf, *Chem. Rev.*, 2017, **117**, 1319–1406.
7 S. Nazhat, S. Parker, M. Patel and M. Braden, *Biomaterials*, 2001, **22**, 2411–2416.
8 W. H. Kaminsky and B., *Plast. Eng.*, 2005, **70**, 333–380.
9 *A. Region Europe, And Segment Forecasts, 2021–2028*.
10 S. Förster and E. Krämer, *Macromolecules*, 1999, **32**, 2783–2785.
11 J. K. Wegrzyn, T. Stephan, R. Lau and R. B. Grubbs, *J. Polym. Sci., Part A: Polym. Chem.*, 2005, **43**, 2977–2984.
12 J. W. Bartels, S. I. Cauët, P. L. Billings, L. Y. Lin, J. Zhu, C. Fidge, D. J. Pochan and K. L. Wooley, *Macromolecules*, 2010, **43**, 7128–7138.
13 S. C. Schmidt and M. A. Hillmyer, *Macromolecules*, 1999, **32**, 4794–4801.
14 J. Wootthikanokkhan and B. Tongrubbai, *J. Appl. Polym. Sci.*, 2003, **88**, 921–927.
15 K. S. Murthy, Q. Ma, E. E. Remsen, T. Kowalewski and K. L. Wooley, *J. Mater. Chem.*, 2003, **13**, 2785–2795.
16 C. Cheng, K. Qi, E. Khoshdel and K. L. Wooley, *J. Am. Chem. Soc.*, 2006, **128**, 6808–6809.
17 D. Vinciguerra, A. Degrassi, L. Mancini, S. Mura, J. Mougin, P. Couvreur and J. Nicolas, *Biomacromolecules*, 2019, **20**, 2464–2476.
18 D. Vinciguerra, M. Jacobs, S. Denis, J. Mougin, Y. Guillaneuf, G. Lazzari, C. Zhu, S. Mura, P. Couvreur and J. Nicolas, *J. Controlled Release*, 2019, **295**, 223–236.
19 S. Harrison, J. Nicolas, A. Maksimenko, D. T. Bui, J. Mougin and P. Couvreur, *Angew. Chem., Int. Ed.*, 2013, **52**, 1678–1682.
20 Y. Bao, E. Guégain, V. Nicolas and J. Nicolas, *Chem. Commun.*, 2017, **53**, 4489–4492.
21 Y. Bao, E. Guégain, J. Mougin and J. Nicolas, *Polym. Chem.*, 2018, **9**, 687–698.
22 Y. Bao, T. Boissenot, E. Guégain, D. Desmaële, S. Mura, P. Couvreur and J. Nicolas, *Chem. Mater.*, 2016, **28**, 6266–6275.

23 S. Schlögl, M.-L. Trutschel, W. Chassé, I. Letofsky-Papst, R. Schaller, A. Holzner, G. Riess, W. Kern and K. Saalwächter, *Polymer*, 2014, **55**, 5584–5595.
24 W. M. Gramlich and M. A. Hillmyer, *Polym. Chem.*, 2011, **2**, 2062–2067.
25 F. Chen and J. Qian, *Fuel*, 2002, **81**, 2071–2077.
26 S.-Y. Chen, Y. Huang and R. C.-C. Tsiang, *J. Polym. Sci., Part A: Polym. Chem.*, 2008, **46**, 1964–1973.
27 E. I. Baptista, G. M. Campese, N. L. Zalloum, A. F. Rubira and E. C. Muniz, *Polym. Degrad. Stab.*, 1998, **60**, 309–315.
28 P. Berto, S. Grelier and F. Peruch, *Polym. Degrad. Stab.*, 2018, **154**, 295–303.
29 C. W. Phetphaisit and P. Phinyocheep, *J. Appl. Polym. Sci.*, 2003, **90**, 3546–3555.
30 S. S. Solanky, I. Campistron, A. Laguerre and J.-F. Pilard, *Macromol. Chem. Phys.*, 2005, **206**, 1057–1063.
31 S. Ouardad and F. Peruch, *Polym. Degrad. Stab.*, 2014, **99**, 249–253.
32 J. A. Blach, G. S. Watson, W. K. Busfield and S. Myhra, *Polym. Int.*, 2002, **51**, 12–20.
33 C. Adam, J. Lacoste and J. Lemaire, *Polym. Degrad. Stab.*, 1991, **32**, 51–69.
34 S. Sato, Y. Honda, M. Kuwahara and T. Watanabe, *Biomacromolecules*, 2003, **4**, 321–329.
35 M. Enoki, Y. Doi and T. Iwata, *Macromol. Biosci.*, 2003, **3**, 668–674.
36 A.-L. Altenhoff, S. Thierbach and A. Steinbüchel, *Biodegradation*, 2021, **32**, 113–125.
37 M. D. Chengalroyen and E. R. Dabbs, *J. Polym. Environ.*, 2013, **21**, 874–880.
38 A. Tardy, N. Gil, C. M. Plummer, C. Zhu, S. Harrisson, D. Siri, J. Nicolas, D. Gigmes, Y. Guillaneuf and C. Lefay, *Polym. Chem.*, 2020, **11**, 7159–7169.
39 N. M. Bingham and P. J. Roth, *Chem. Commun.*, 2019, **55**, 55–58.
40 R. A. Smith, G. Fu, O. McAteer, M. Xu and W. R. Gutekunst, *J. Am. Chem. Soc.*, 2019, **141**, 1446–1451.
41 N. M. Bingham, Q. U. Nisa, S. H. L. Chua, L. Fontugne, M. P. Spick and P. J. Roth, *ACS Appl. Polym. Mater.*, 2020, **2**, 3440–3449.
42 N. Gil, B. Caron, D. Siri, J. Roche, S. Hadiouch, D. Khedaioui, S. Ranque, C. Cassagne, D. Montarnal and D. Gigmes, *Macromolecules*, 2022, **55**, 6680–6694.
43 M. P. Spick, N. M. Bingham, Y. Li, J. de Jesus, C. Costa, M. J. Bailey and P. J. Roth, *Macromolecules*, 2020, **53**, 539–547.
44 P. Galanopoulo, N. Gil, D. Gigmes, C. Lefay, Y. Guillaneuf, M. Lages, J. Nicolas, M. Lansalot and F. D'Agosto, *Angew. Chem., Int. Ed.*, 2022, **61**, e202117498.
45 N. Gil, C. Thomas, R. Mhanna, J. Mauriello, R. Maury, B. Leuschel, J.-P. Malval, J.-L. Clément, D. Gigmes and C. Lefay, *Angew. Chem., Int. Ed.*, 2021, **134**, e202117700.
46 M. Lages, N. Gil, P. Galanopoulo, J. Mougin, C. Lefay, Y. Guillaneuf, M. Lansalot, F. D'Agosto and J. Nicolas, *Macromolecules*, 2022, **55**, 9790–9801.
47 G. R. Kiel, D. J. Lundberg, E. Prince, K. E. L. Husted, A. M. Johnson, V. Lensch, S. Li, P. Shieh and J. A. Johnson, *J. Am. Chem. Soc.*, 2022, **144**, 12979–12988.

48 N. Bingham, Q. Nisa, P. Gupta, N. Young, E. Velliou and P. Roth, *Biomacromolecules*, 2022, **23**, 2031–2039.

49 J. Nicolas, Y. Guillaneuf, C. Lefay, D. Bertin, D. Gigmes and B. Charleux, *Prog. Polym. Sci.*, 2013, **38**, 63–235.

50 S. Perrier, *Macromolecules*, 2017, **50**, 7433–7447.

51 M. R. Wood, D. J. Duncalf, S. P. Rannard and S. Perrier, *Org. Lett.*, 2006, **8**, 553–556.

52 S. Allorio, S. Pispas, E. Siakali-Kioulafa and N. Hadjichristidis, *J. Polym. Sci., Part B: Polym. Phys.*, 1995, **33**, 2229–2234.

53 S. Harrisson, P. Couvreur and J. Nicolas, *Macromolecules*, 2011, **44**, 9230–9238.

54 M. Van Den Brink, A. M. Van Herk and A. L. German, *J. Polym. Sci., Part A: Polym. Chem.*, 1999, **37**, 3793–3803.

55 S. Harrisson, P. Couvreur and J. Nicolas, *Macromol. Rapid Commun.*, 2012, **33**, 805–810.

56 V. Jitchum and S. Perrier, *Macromolecules*, 2007, **40**, 1408–1412.

57 V. Delplace, S. Harrisson, A. Tardy, D. Gigmes, Y. Guillaneuf and J. Nicolas, *Macromol. Rapid Commun.*, 2014, **35**, 484–491.

58 D. Gigmes, P. H. M. Van Steenberge, D. Siri, D. R. D'hooge, Y. Guillaneuf and C. Lefay, *Macromol. Rapid Commun.*, 2018, **39**, 1800193.

59 O. Ivanchenko, S. Mazières, S. Harrisson and M. Destarac, *Polym. Chem.*, 2022, **13**, 5525–5529.

60 C. Vauthier, C. Dubernet, E. Fattal, H. Pinto-Alphandary and P. Couvreur, *Adv. Drug Delivery Rev.*, 2003, **55**, 519–548.

61 A. Kumari, S. K. Yadav and S. C. Yadav, *Colloids Surf., B*, 2010, **75**, 1–18.

62 E. M. Pridgen, R. Langer and O. C. Farokhzad, *Nanomedicine*, 2007, **2**, 669–680.

63 K. S. Soppimath, T. M. Aminabhavi, A. R. Kulkarni and W. E. Rudzinski, *J. Controlled Release*, 2001, **70**, 1–20.

64 M. Sumana, A. Thirumurugan, P. Muthukumaran and K. Anand, in *Integrative Nanomedicine for New Therapies*, Springer, 2020, pp. 231–246.

65 V. Delplace, P. Couvreur and J. Nicolas, *Polym. Chem.*, 2014, **5**, 1529–1544.

66 I. Ekladious, Y. L. Colson and M. W. Grinstaff, *Nat. Rev. Drug Discovery*, 2019, **18**, 273–294.

67 M. L. Girase, P. G. Patil and P. P. Ige, *Int. J. Polym. Mater. Polym. Biomater.*, 2020, **69**, 990–1014.

68 P. Thakor, V. Bhavana, R. Sharma, S. Srivastava, S. B. Singh and N. K. Mehra, *Drug Discovery Today*, 2020, **25**, 1718–1726.

69 J. Nicolas, *Chem. Mater.*, 2016, **28**, 1591–1606.

70 Y. Bao and J. Nicolas, *Polym. Chem.*, 2017, **8**, 5174–5184.

71 E. Guégain, J. Tran, Q. Deguettes and J. Nicolas, *Chem. Sci.*, 2018, **9**, 8291–8306.

72 D. Vinciguerra, S. Denis, J. Mougin, M. Jacobs, Y. Guillaneuf, S. Mura, P. Couvreur and J. Nicolas, *J. Controlled Release*, 2018, **286**, 425–438.

73 C. S. Gondi and J. S. Rao, *Expert Opin. Ther. Targets*, 2013, **17**, 281–291.

74 D. Dheer, J. Nicolas and R. Shankar, *Adv. Drug Delivery Rev.*, 2019, **151–152**, 130–151.

75 P. Gao, J. Nicolas and T. Ha-Duong, *J. Am. Chem. Soc.*, 2021, **143**, 17412–17423.

76 V. Heinemann, Y.-Z. Xu, S. Chubb, A. Sen, L. W. Hertel, G. B. Grindey and W. Plunkett, *Cancer Res.*, 1992, **52**, 533–539.

77 G. G. Hedir, C. A. Bell, N. S. Ieong, E. Chapman, I. R. Collins, R. K. O'Reilly and A. P. Dove, *Macromolecules*, 2014, **47**, 2847–2852.

78 G. G. Hedir, C. A. Bell, R. K. O'Reilly and A. P. Dove, *Biomacromolecules*, 2015, **16**, 2049–2058.

79 C. Zhu, S. Denis and J. Nicolas, *Chem. Mater.*, 2022, **34**, 1875–1888.

80 V. Delplace, E. Guégain, S. Harrisson, D. Gigmes, Y. Guillaneuf and J. Nicolas, *Chem. Commun.*, 2015, **51**, 12847–12850.

81 J. Undin, A. Finne-Wistrand and A.-C. Albertsson, *Biomacromolecules*, 2014, **15**, 2800–2807.

82 E. Guégain, J.-P. Michel, T. Boissenot and J. Nicolas, *Macromolecules*, 2018, **51**, 724–736.

83 J. Tran, T. Pesenti, J. Cressonnier, C. Lefay, D. Gigmes, Y. Guillaneuf and J. Nicolas, *Biomacromolecules*, 2019, **20**, 305–317.